

Finite element models with node-dependent kinematics for the analysis of composite beam structures

*Original*

Finite element models with node-dependent kinematics for the analysis of composite beam structures / Carrera, E.; Zappino, E.; Li, G.. - In: COMPOSITES. PART B, ENGINEERING. - ISSN 1359-8368. - 132:(2018), pp. 35-48. [10.1016/j.compositesb.2017.08.008]

*Availability:*

This version is available at: 11583/2692893 since: 2017-11-20T17:27:37Z

*Publisher:*

Elsevier Ltd

*Published*

DOI:10.1016/j.compositesb.2017.08.008

*Terms of use:*

This article is made available under terms and conditions as specified in the corresponding bibliographic description in the repository

*Publisher copyright*

Elsevier postprint/Author's Accepted Manuscript

© 2018. This manuscript version is made available under the CC-BY-NC-ND 4.0 license  
<http://creativecommons.org/licenses/by-nc-nd/4.0/>. The final authenticated version is available online at:  
<http://dx.doi.org/10.1016/j.compositesb.2017.08.008>

(Article begins on next page)

# Finite Element Models with Node-dependent Kinematics for the Analysis of Composite Beam Structures

E. Carrera, E. Zappino, and G. Li

*MUL*<sup>2</sup> Group, Department of Mechanical and Aerospace Engineering, Politecnico di Torino,  
Corso Duca degli Abruzzi 24, 10129 Torino, Italy.

*Keywords:*

beam element, Carrera Unified Formulation, global-local analysis, node-dependent kinematics.

*Author and address for Correspondence*

Dr. Enrico Zappino  
Department of Mechanical and Aerospace Engineering  
Politecnico di Torino,  
Corso Duca degli Abruzzi, 24,  
10129 Torino, ITALY,  
Tel: +39 0110906887, Fax: +39 0110906899  
E-mail: enrico.zappino@polito.it

## Abstract

This paper presents refined one-dimensional models with node-dependent kinematics. The three-dimensional displacement field is discretized into two domains, namely cross-section domain and axis domain. The mechanical behaviors of the beam can be firstly captured by the cross-section functions then interpolated by the nodal shape functions of the beam element. Such a feature makes it possible to adopt different types of cross-section functions on each element node, obtaining node-dependent kinematic finite element models. Such models can integrate Taylor-based and Lagrange-type nodal kinematics on element level, bridging a less-refined model to a more refined model without using special coupling methods. FE governing equations of node-dependent models are derived by applying the Carrera Unified Formulation. Some numerical cases on metallic and composite beam-like structures are studied to demonstrate the effectiveness of node-dependent models in bridging a locally refined model to a global model when local effects should be accounted for.

## 1 Introduction

Application of composite materials has attracted significant attention over the past several decades to improve the structural efficiency. However, the anisotropy of multi-layered structures makes it computational costly to capture their responses under external loads.

One of the most important issues in numerical modeling is saving computational costs. A major approach is only using refined higher-order models in regions where sophisticated effects have to be described, while employing less refined models in the rest of the structure. Some noticeable methods have been proposed to couple different models. Slender structures can be approximated with beam models. The most classical beam model is Euler-Bernoulli beam, which applies to isotropic beam-like structures with high slenderness ratio. For stubby beam-like structures the shear effects can be captured with Timoshenko [1] beam model. However, to better capture the behavior of composite laminated beams, more reliable models are needed.

Over the last several decades, many refined beam models have been proposed. To consider the deformation of cross-sections, Vlasov [2] proposed the use of warping functions for beam models, this approach has been applied by Friberg [3], Ambrosini *et al.* [4] and Mechab *et al.* [5] to capturing the key phenomenon of cross-sectional warping of thin-walled structures. Kim and Lee [6] recently applied a hybrid model based on Euler-Bernoulli and Vlasov models to the study of thin-walled beam including functionally graded materials. Schardt [7] proposed Generalized Beam Theory (GBT) by expanding the displacement field with reference to the mid-plane of the cross-section thin-walled beam. GBT was also adopted by Davies and Leach [8] and Davies *et al.* [9], and then further extension to the analysis of composite structures was proposed by Silvestre and Camotim [10]. Berdichevsky [11] proposed the Variation Asymptotic Method (VAM) which uses a characteristic cross-section parameter to construct an asymptotic expansion of the solution, this approach was also adopted by Giavotto *et al.* [12]. Volovoi *et al.* [13], Yu *et al.* [14] and Yu and Hodges [15] further applied VAM to composite beam-like structures.

Carrera [16] and Carrera *et al.* [17] proposed a new methodology, which is known as Carrera Unified Formulation (CUF), as a new framework to construct 1D and 2D models for the analysis of multi-layered composites. For 1D (beam) models, CUF introduces functions  $F_\tau(x, z)$  (based either on series expansion or interpolation polynomials) to approximate a cross-section. Numerical accuracy can be improved by increasing the number of expansions in a convenient way as demonstrated by Carrera *et al.* [18], while cumbersome derivation of governing equations can be avoided thanks to the introduction of *Fundamental Nucleus*, FN, which is the core unit of the structural stiffness matrix. Such an advantage leads to a variety of models with variable kinematics, including both 1D models by Carrera *et al.* [19] and 2D models by Cinefra *et al.* [20] and Cinefra and Valvano [21].

The above-described refined models improve the numerical accuracy at the expense of increasing the computational costs. For example, CUF-based FE models increase the number of degrees of freedom at each node to better approximate the structural responses. Composite material may undergo to local effects as delamination [22], cracks [23] or local buckling [24], these phenomena require accurate models to be predicted. If refined models are only used in specific regions with sophisticated effects (such as high gradients of stress) to be captured leaving the rest of the structure modeled with lower-order models, a compromise between accuracy and consumption can be reached. The coupling of two computational domains has attracted significant attention, leading to various global-local analysis methods.

To enforce the compatibility of the displacements at the interface of the two domains, Prager [25] used a set of Lagrange multipliers, which was further extended to beam models in the framework of CUF [26]. Aminpour *et al.* [27], and Ransom [28] employed a spline method to couple two domains with different meshes. Similar approaches in the framework of three-field formulation were also reported by Brezzi and Marini [29]. Blanco *et al.* [30, 31] presented an eXtended Variational Formulation (XVF) to couple non-matching kinematic models based on Lagrange multiplier method, which was also adopted by Wenzel *et al.* [32].

Fish *et al.* [33] developed an accelerated multi-grid method to speed up the iterative process when sharing the information between coarse and fine meshes. Fish [34] put forward *s*-version finite element method, which improves the accuracy in the local domain by superimposing additional elements with higher-order hierarchical kinematics on the global model, and continuity of displacement can be guaranteed by imposing homogeneous boundary conditions on the superimposed field. Park *et al.* [35] proposed a similar method which also refines the local mesh without using transition region nor multi-point constraint. The *s*-version FE method was also used in combination with *h*-version [36] and *p*-version models [29], leading to simultaneous multiple model approaches, as summarized by Reddy and Robbins [37] and Reddy [38].

By introducing an overlapping zone to bridge the two domains, Ben Dhia [39] and Ben Dhia and Rateau [40] suggested Arlequin method to impose compatibility within the overlapping domain with Lagrange multipliers. Such an approach has also been implemented in CUF-based models by Biscani *et al.* for beam models [41] and plate models [42, 43]. Hu *et al.* [44, 45] applied Arlequin method in the linear and non-linear multi-scale analysis of sandwich structures. He *et al.* [46] adopted Arlequin method to bridge low- and high-order models constructed in the framework of CUF, and Constrained Variational Principle (CVP) was used to derive beam elements for layered structures with independent kinematic description in each layer.

Some special techniques that can be used to mix elements with different mesh refinement or of different types have also been implemented in commonly used commercial software. In Rigid Beam Element (RBEi) and Multi-Point Constraints (MPCs) (such as in NX NASTRAN), the dependent degrees of freedom are expressed as a linear function of the independent degrees of freedoms. Such approaches can be used to connect two sets of incompatible elements in simultaneous analyses. ABAQUS provides so-called “Shell-to-solid coupling” which allows for a transition from 2D modelling to 3D modelling. This method uses a set of internally defined distributing coupling constraints to connect nodes along the edge of a 2D model to a set of nodes on a solid surface. Submodeling is a two-step technique, in which the local model is driven on the boundaries nodes by the displacement field obtained with an beforehand global model. The drawback of such an approach is that the change of stiffness of the local model cannot be updated in the global model. A superelement can be treated as an individual element that is defined by grouping a set of elements, and *condensing* the so-called internal degrees of freedom. Such a technique suits the analysis of large-scale structures and parallel computation. All these approaches adopt special coupling functions on the interfaces between the local and the global model or employ special matrix operation techniques. Meanwhile, at least two sets of separately meshed models are needed.

CUF-type displacement functions make it possible to implement node-dependent kinematic FE

models. When it comes to refined 1D (beam) models, cross-section functions defined on different nodes can be integrated into the same 1D element by the nodal Lagrangian shape functions. By the introduction of fundamental nucleus, as has been elucidated in [47], the governing equation can be derived and expressed in a compact way. Such a methodology permits the possibility of connecting to domains with different kinematics by commonly used nodal shape functions without using any specially designed coupling methods, which reduces the complexity of the numerical methods significantly. Such an approach was firstly presented by Carrera and Zappino [48], then extended to the global-local analysis of laminated composite plates by Zappino et al. [49] as well as [50]. As a simplified case, through-the-thickness variable kinematics was discussed by Dehkordi et al. [51] for sandwich plates, and by Carrera et al. [52] for laminated shells.

In the present work, node-dependent kinematic one-dimensional models are applied to construct global-local FE models, and special attention is paid to the analysis of composite structures where the use of refined models is mandatory to obtain accurate results. The governing equations for beam models with node-dependent kinematics are firstly derived by applying Principle of Virtual Displacement (PVD). Numerical results on thin-walled isotropic beam and multi-layered composite beam, as well as a composite thin-walled beam are reported.

## 2 Preliminaries

Consider a slender structure as shown in Fig. 1, in which the axial direction is along the  $y$  direction, the displacement vector can be expressed as:

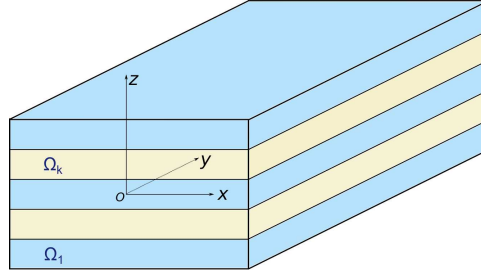


Figure 1: Reference system of a laminated beam model.

$$\mathbf{u}^T = \{u_x(x, y, z), u_y(x, y, z), u_z(x, y, z)\} \quad (1)$$

where  $u_x, u_y$  and  $u_z$  are the three displacement components. The strain and stress components are arranged as follows:

$$\boldsymbol{\epsilon}^T = \{\epsilon_{xx}, \epsilon_{yy}, \epsilon_{zz}, \epsilon_{xz}, \epsilon_{yz}, \epsilon_{yx}\} \quad (2)$$

$$\boldsymbol{\sigma}^T = \{\sigma_{xx}, \sigma_{yy}, \sigma_{zz}, \sigma_{xz}, \sigma_{yz}, \sigma_{yx}\} \quad (3)$$

The strain vector  $\boldsymbol{\epsilon}_p$  and  $\boldsymbol{\epsilon}_n$  can be obtained via the geometrical equation:

$$\boldsymbol{\epsilon} = \mathbf{D}\mathbf{u} \quad (4)$$

the explicit expressions of the differential operator matrices are as follows:

$$\mathbf{D} = \begin{bmatrix} \frac{\partial}{\partial x} & 0 & 0 \\ 0 & \frac{\partial}{\partial y} & 0 \\ 0 & 0 & \frac{\partial}{\partial z} \\ \frac{\partial}{\partial z} & 0 & \frac{\partial}{\partial x} \\ 0 & \frac{\partial}{\partial z} & \frac{\partial}{\partial y} \\ \frac{\partial}{\partial y} & \frac{\partial}{\partial x} & 0 \end{bmatrix} \quad (5)$$

The stress components can be attained by means of the constitutive equation as follows:

$$\boldsymbol{\sigma} = \tilde{\mathbf{C}}\boldsymbol{\epsilon} \quad (6)$$

where  $\tilde{\mathbf{C}}$ , is the matrix of the material coefficients defined in the general physical system  $(x, y, z)$  rotated from the material coordinate system (1,2,3), and their explicit expressions can be found in [53].

### 3 Refined one-dimensional models

One-dimensional models describe kinematics of beam-like slender structures with cross-section functions  $F_\tau(x, z)$  and axial displacement functions  $\mathbf{u}_\tau(y)$ , and in a compact way the displacement field can be approximated with the following displacement functions:

$$\mathbf{u} = \mathbf{u}_\tau(y)F_\tau(x, z), \quad \tau = 1, \dots, M \quad (7)$$

where  $F_\tau(x, z)$  are the expanded functions over the cross-section domain defined on  $(x, y)$ , and  $\mathbf{u}_\tau(y)$  is the unknown vector along the axis of the beam.  $M$  is the number of expansion terms used to describe the cross-section behavior. Both series expansion theories and interpolation polynomials can be described in such a framework. When applied to FE models, the axial displacement function  $\mathbf{u}_\tau$  can be approximated by the nodal Lagrangian shape functions  $N_i(y)$ , namely:

$$\mathbf{u} = N_i(y)F_\tau(x, z)\mathbf{u}_{i\tau}, \quad \tau = 1, \dots, M; \quad i = 1, \dots, N_n \quad (8)$$

in which  $N_i(y)$  is the shape function of node  $i$ , and  $N_n$  is the number of nodes in an element.  $\mathbf{u}_{i\tau}$  is the vector of nodal unknowns, or mathematically weighting factors of the expansion terms. Correspondingly the virtual variation of the displacement can be written as:

$$\delta\mathbf{u} = N_j(y)F_s(x, z)\delta\mathbf{u}_{js} \quad s = 1, \dots, M; \quad j = 1, \dots, N_n. \quad (9)$$

A variety of theories can be implemented with CUF and the fundamental nucleus can be adjusted to different theories conveniently. In the context of composite laminates, CUF can be used to describe Equivalent Single Layer (ESL) models with series expansions, and Layer-Wise (LW) models with interpolation polynomials. The most commonly used theories are Taylor series and Lagrange expansions, which are also adopted in the analysis reported in the following sections.

#### 3.1 Taylor expansion models (TE)

The one-dimensional models based on Taylor Expansions (TE) use function series with the form  $x^m z^n$  (where  $m$  and  $n$  are positive integers) to describe the kinematics over the cross-section. Taking a set of displacement functions of the second order as an example, the displacement field is assumed to be as following:

$$\begin{cases} u_x = u_{x_1} + xu_{x_2} + zu_{x_3} + x^2u_{x_4} + xzu_{x_5} + z^2u_{x_6} \\ u_y = u_{y_1} + xu_{y_2} + zu_{y_3} + x^2u_{y_4} + xzu_{y_5} + z^2u_{y_6} \\ u_z = u_{z_1} + xu_{z_2} + zu_{z_3} + x^2u_{z_4} + xzu_{z_5} + z^2u_{z_6} \end{cases} \quad (10)$$

in which the series expansion  $F_\tau$  are:

$$F_1 = 1, \quad F_2 = x, \quad F_3 = z, \quad F_4 = x^2, \quad F_5 = xz, \quad F_6 = z^2 \quad (11)$$

TE models can be represented by **TE** $n$ , where  $n$  indicates the highest order of the polynomials adopted. Timoshenko and Euler-Bernoulli beam theories can be treated as a particular case of TE model.

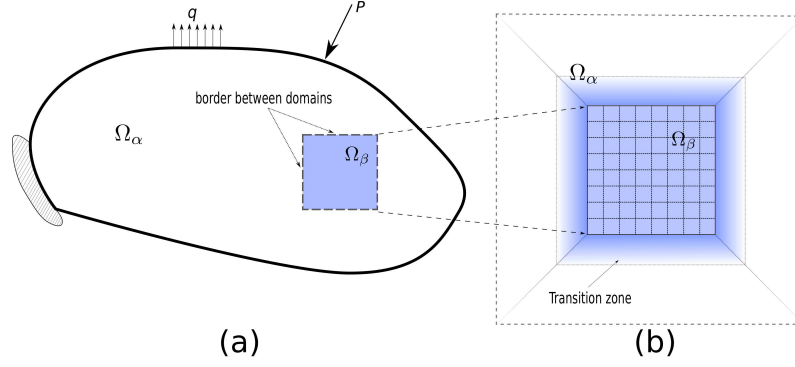


Figure 2: Global-local method.

### 3.2 Lagrange expansion models (LE)

Lagrange interpolation polynomials can also be adopted as cross-section functions, leading to **LE** models. The displacement field of a quadrilateral cross-section can be assumed as:

$$\begin{aligned} F_1 &= \frac{1}{4}(1 - \xi)(1 - \eta); & F_2 &= \frac{1}{4}(1 + \xi)(1 - \eta); \\ F_3 &= \frac{1}{4}(1 + \xi)(1 + \eta); & F_4 &= \frac{1}{4}(1 - \xi)(1 + \eta). \end{aligned} \quad (12)$$

where  $\xi$  and  $\eta$  are the coordinates in the natural reference system of a quadrilateral element, that is  $F_1(-1, -1) = 1$ ,  $F_2(1, -1) = 1$ ,  $F_3(1, 1) = 1$ , and  $F_4(-1, 1) = 1$ . When displacement-based LE models are employed, the degrees of freedom of the FE models are the physical displacement of the nodes (interpolation points). With LE4 and LE9 are denoted the four- and the nine-node element respectively, about which more details can be found in [17] and in [47].

## 4 CUF-based beam element with node-dependent kinematics

FE subdivides the whole domain into elements (sub-domains) to approximate the displacement field. In each element domain, based on the interpolation among a set of nodes, the displacement field can be approximated. Usually to save the computational costs, engineers tends to use detailed models only within those regions of interest (such as constrained ends, loaded surfaces or regions with other local effects like embed components), which can be denoted as  $\Omega_\beta$  in Figure Fig. 2(a), and employ less-refined mesh or low order models in the outer region  $\Omega_\alpha$ .

Distinguished from the coupling methods discussed in the introduction, in this section an innovative approach to obtain variable kinematic models based on the CUF is presented. Instead of using an overlap between the two domains, node dependent kinematic elements are used to connect zones with different kinematics, as shown in Fig. 2(b). Within the transition zone, the elements employ node-dependent kinematics, which means that the kinematic description on each node is independent and a natural kinematic variation can be realized over the domain of an element. The kinematic variation can be achieved with the commonly used Lagrangian shape functions, which avoids any *ad hoc* assumption and leads to advanced models with compact FE formulations.

In the context of one-dimensional FE modeling, to approximate a cantilever beam with localized effects to be considered at the free end, as shown in Fig. 3, refined models can be used only in the local region, and connected to the rest part by a bridging zone. This approach allows the computational costs to be reduced. According to the one-dimensional displacement approximation, see Eq. (9) and Eq. (8), the mechanical behavior of the cross-section associated at the node  $i$  is approximate by the corresponding cross-section expansion  $F_\tau(x, z)$ , then interpolate over the beam axis by the FE shape functions

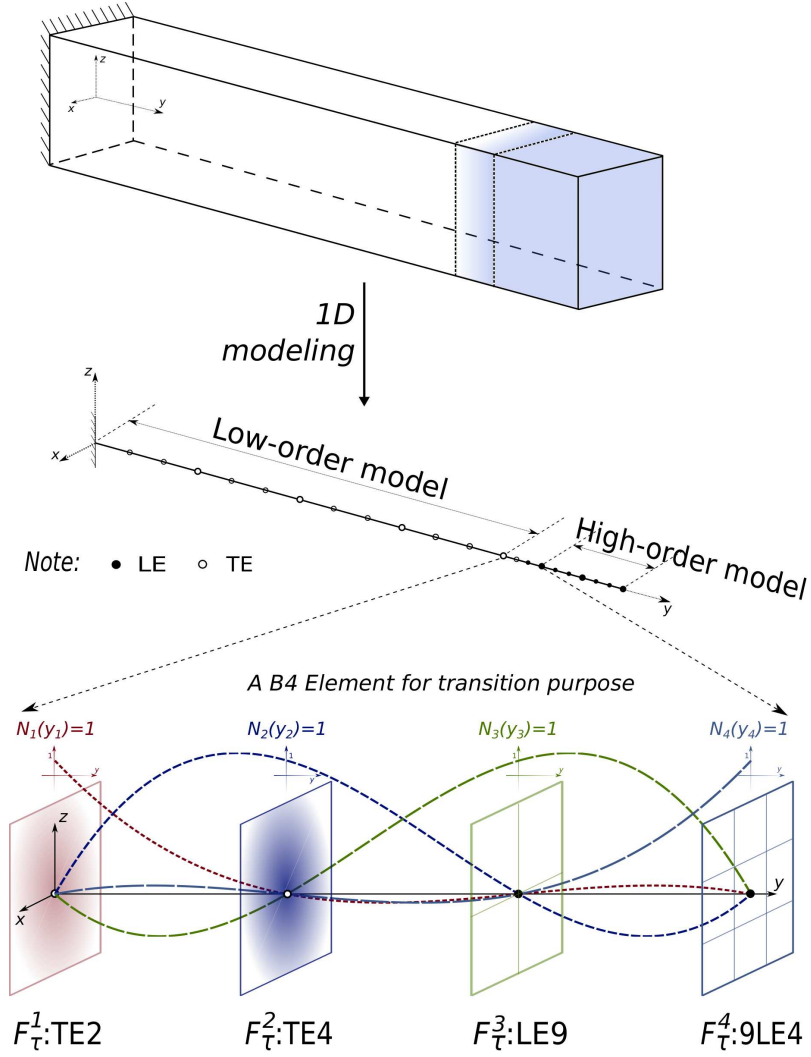


Figure 3: A CUF-based B4 element for transition with node-dependent kinematics.

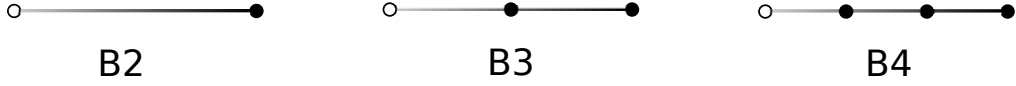
$N_i(y)$ . If  $F_{\tau}(x, z)$  is further related to the node  $i$ , leading to node-dependent cross-section kinematics  $F_{\tau}^i(x, y)$ , thus the displacement field of the node-dependent kinematic one-dimensional models can be expressed as follows:

$$\mathbf{u}(x, y, z) = N_i(y) \cdot F_{\tau}^i(x, z) \cdot \mathbf{U}_{i_{\tau}} \quad (13)$$

When a B4 element is considered, as shown in Fig. 3 as an example, on each of the four nodes a different cross-section approximation can be adopted (namely TE2, TE4, LE9 and 9LE4, respectively). Here a L9 refers to a nine-nodes quadrilateral element; while 9LE4 indicates 9 quadrilateral sub-domains on the cross-section, each described by a four-node Lagrangian element. The nodal kinematics are further integrated by the FE Lagrangian shape functions  $N_i(y)$  to construct an element for transition purpose. Such a bridging method can naturally lead to continuous displacement field.

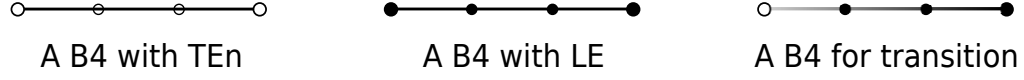
Simpler cases can be B2 or B3 elements with a lower number of cross-section functions, as shown in Fig. 4. The cross-section functions associated to each node can be assumed to be any applicable theory. For the purpose of transition, higher-order theories can be used on the side connected to the local model, while lower-order models on the side lies in the outer region. In this work, TE and LE models are mainly discussed in the numerical cases, leading to B4 elements as shown in Fig. 5.





Note: • High-order kinematics    ◦ Low-order kinematics

Figure 4: Variable kinematic elements: B2, B3 and B4.



Note: • LE    ◦ TE

Figure 5: Three types of B4 elements used in the FE model.

#### 4.1 FE governing equations

The governing equations are derived by applying the Principal of Virtual Displacements (PVD). For a static problem:

$$\delta L_{int} = \delta L_{ext} \quad (14)$$

where  $L_{int}$  represents the strain energy due to the deformation, and  $L_{ext}$  stands for the work done by the external loads on the virtual displacement.  $\delta$  indicates the virtual variation. The internal work can be expressed as:

$$\delta L_{int} = \int_V \delta \epsilon^T \sigma dV \quad (15)$$

By introducing the displacement description Eq. (13), the geometrical relations Eq. (4) and the constitutive equations Eq. (6), the variation on internal work can be written as:

$$\delta L_{int} = \delta \mathbf{u}_{js}^T \cdot \int_V N_j F_s^j \mathbf{D}^T \mathbf{C} \mathbf{D} F_\tau^i N_i dV \cdot \mathbf{u}_{i\tau} = \delta \mathbf{u}_{js}^T \cdot \mathbf{K}^{ij\tau s} \cdot \mathbf{u}_{i\tau} \quad (16)$$

in which  $\mathbf{K}^{ij\tau s}$  is a  $3 \times 3$  matrix, which is also known as *fundamental nucleus* in the context of CUF, acting as the core unit of the stiffness matrix. By applying the Einstein's summation convention, the element stiffness matrix can be constructed.  $\mathbf{u}_{i\tau}$  and  $\delta \mathbf{u}_{js}$  are the displacement vector and its virtual variation. The explicit expression of  $\mathbf{K}^{ij\tau s}$  has been given in Appendix.

Considering the work done by the external load  $\mathbf{p}$ , the virtual variation of external work can be expressed as:

$$\delta L_{ext} = \int_V \delta \mathbf{u}^T \mathbf{p} dV \quad (17)$$

By introducing the displacement functions Eq. (13), one can obtain:

$$\delta L_{ext} = \delta \mathbf{u}_{js}^T \int_V N_j F_s^j \mathbf{p} dV = \delta \mathbf{u}_{js}^T \mathbf{P}^{js} \quad (18)$$

where  $\mathbf{P}^{js}$  is the expression of the load vector. Thus, the governing equation can be written as:

$$\delta \mathbf{u}_{js} : \quad \mathbf{K}^{ij\tau s} \cdot \mathbf{u}_{i\tau} = \mathbf{P}^{js} \quad (19)$$

#### 4.2 Assembly of the stiffness matrix

As has been discussed in the above section, the *fundamental nucleus* is a core unit of the stiffness matrix. By looping on the superscripts, the stiffness matrix on node and element level can be obtained,

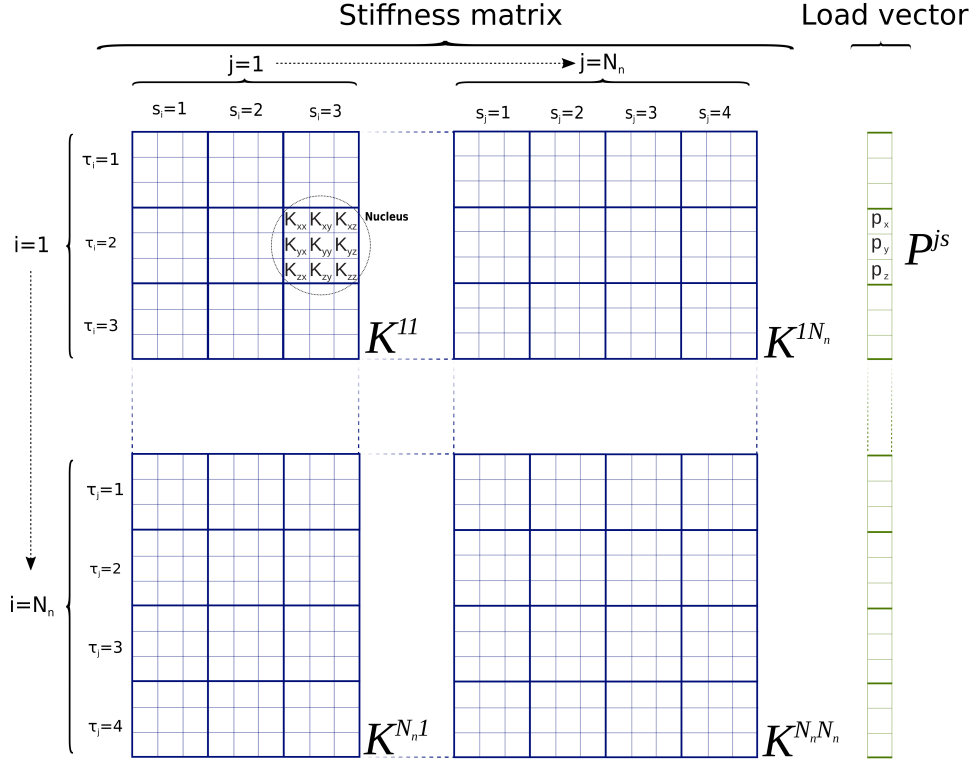


Figure 6: Assembly of the stiffness matrix and load vector of models with node-dependent kinematics.

then further assembled on the structure level. Such an assembly technique has been elaborated in the authors' former work [47].

When various node-dependent kinematics are used on different nodes within one element, considering a general unit of the stiffness matrix  $K^{ij}$ , if  $M_i \neq M_j$ ,  $K^{ij}$  would be rectangular rather than square. For example, if the number of expansion terms on node  $i$  is  $M_i = 3$ , while  $M_j = 4$ , then the dimension of  $K^{ii}$  is  $9 \times 9$ ,  $K^{jj}$  is a  $12 \times 12$  matrix and  $K_{ij}$  is a  $9 \times 12$  while  $K_{ji}$  a  $12 \times 9$ . In a more explicit form, the shapes of these four matrices have been illustrated in Fig. 6. The shape of the load vector should be compatible with the stiffness matrix, as shown in Fig. 6.

## 5 Numerical results

In this section results of three numerical cases obtained with node-dependent kinematic beam models are reported. The first numerical case is an isotropic thin-walled C-section beam, and the following two include an eight-layered composite beam and a one-cell thin-walled composite beam. In all the cases, point loads are imposed to the structures, which lead to strong local stress concentration. Displacements and/or stresses are evaluated in the vicinity of the loading points. The regions that adopt refined models are chosen as: a) in and near the loaded area; b) in and near the constrained region; c) in the area of interest. The structures analyzed are discretized into B4 elements along the axis direction. FE models with node-dependent kinematics are denoted by  $\mathbf{LE}^{\times a}\text{-}\mathbf{TE}^{n \times b}$ , where the superscripts stand for the number of beam elements adopting the corresponding kinematics. Comparisons are made among results obtained with models adopting a) uniform Lagrange expansions; b) full Taylor expansions; and c) variable nodal LE/TE kinematics. In each numerical case only one set of FE mesh is used, and the local model is refined by adopting higher-order nodal kinematics, which is one of the major advantages over traditional global-local approaches.

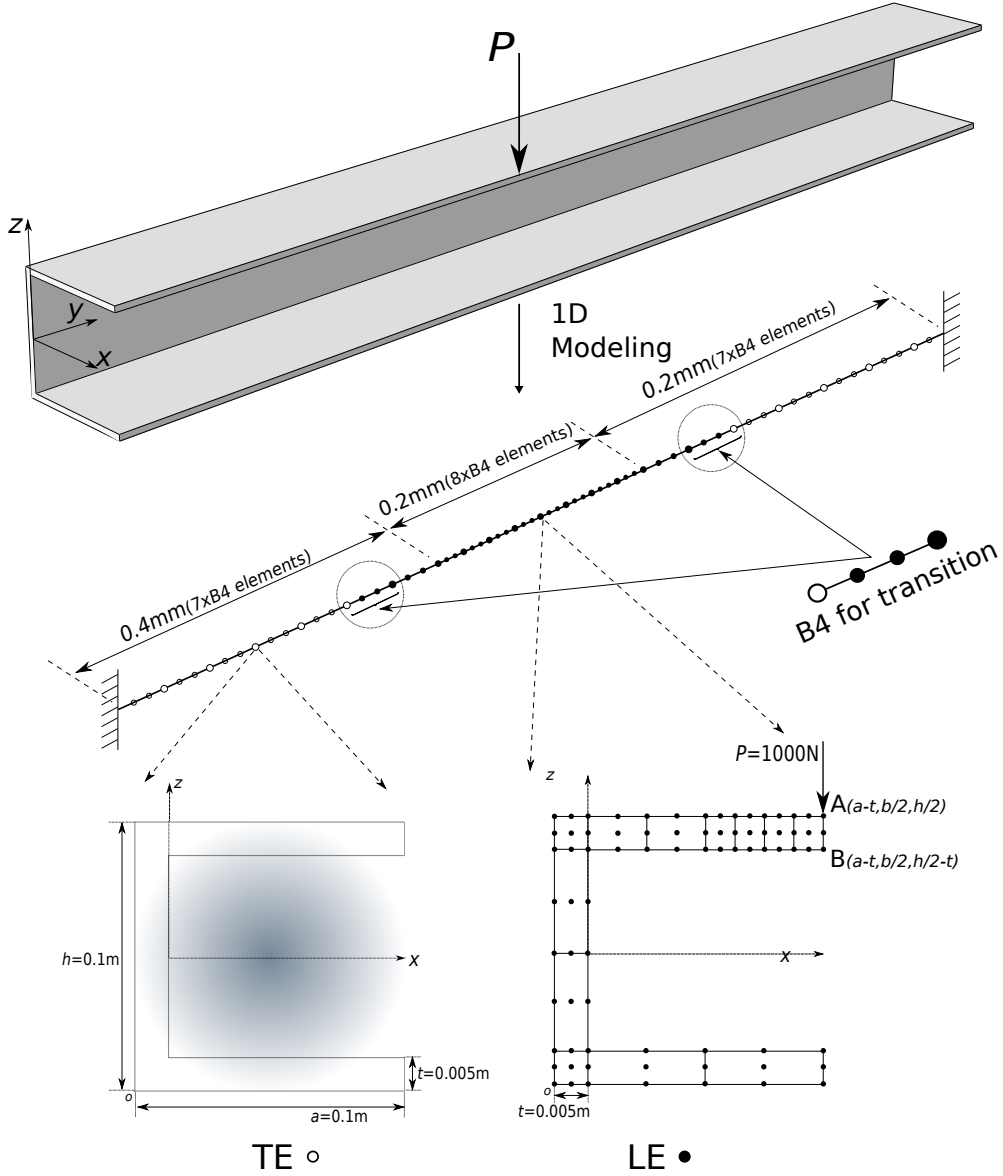


Figure 7: FE discretization of the isotropic beam with node-dependent kinematics.

### 5.1 A thin-walled isotropic beam with C-shaped cross-section

Firstly, an isotropic thin-walled beam-like structure with a C-shaped cross-section is considered. The used material is aluminum alloy, which has a Young modulus  $E = 71.7\text{GPa}$  and Poisson's ratio,  $\nu = 0.3$ . The structure is clamped at two ends and loaded by a concentrated load  $P = 1000\text{N}$  at point  $A(a - t, \frac{b}{2}, \frac{h}{2})$  as shown in Fig. 7. Fig. 7 also illustrates that the structure is discretized into twenty-two B4 elements, including two B4 elements to connect the local inner region with stress field of high gradient to the outer zone. In the inner region refined models with LE models are used, while in the outer area Taylor-based kinematics, TE, are adopted. Three groups of node-dependent kinematic models are used, they use 13, 9, and 5 elements respectively in the central area where local effects are expected. This implies a large, a middle-size and a small zone where refined beam models are used.

Accordingly, the three groups of FE models are denoted as  $\text{LE}^{\times 13}\text{-TE}n^{\times 7}$ ,  $\text{LE}^{\times 9}\text{-TE}n^{\times 11}$ , and  $\text{LE}^{\times 5}\text{-TE}n^{\times 15}$ . To better capture the local stress field, when LE kinematics are adopted, the domain sub-division near the loading point is refined. The evaluation of displacement  $w$  and  $\sigma_{yy}$  at point  $B(a -$

Table 1: Displacement and stress evaluation of the thin-walled isotropic beam.

Model	w[mm]	$\sigma_{yy}[10^2\text{MPa}]$	DOFs
	$B(a-t, \frac{b}{2}, \frac{h}{2}-t)$	$B(a-t, \frac{b}{2}, \frac{h}{2}-t)$	
ABAQUS-3D	-3.441	2.598	924399
LE	-3.326	2.180	15075
TE2	-0.04912	-0.02217	1206
TE3	-0.09333	0.07481	2010
TE4	-0.5705	0.5681	3015
TE5	-0.7969	1.039	4221
TE6	-1.817	1.787	5628
TE7	-2.248	1.646	7236
TE8	-2.487	1.867	9045
LE $\times$ 13-TE2 $\times$ 7	-2.941	2.130	9693
LE $\times$ 13-TE3 $\times$ 7	-3.011	2.143	10005
LE $\times$ 13-TE4 $\times$ 7	-3.227	2.174	10395
LE $\times$ 13-TE5 $\times$ 7	-3.242	2.174	10963
LE $\times$ 13-TE6 $\times$ 7	-3.291	2.178	11409
LE $\times$ 13-TE7 $\times$ 7	-3.309	2.180	12033
LE $\times$ 13-TE8 $\times$ 7	-3.317	2.180	12735
LE $\times$ 9-TE3 $\times$ 11	-2.378	2.155	7665
LE $\times$ 9-TE4 $\times$ 11	-2.767	2.204	8235
LE $\times$ 9-TE5 $\times$ 11	-2.857	2.199	8919
LE $\times$ 9-TE6 $\times$ 11	-3.129	2.188	9717
LE $\times$ 9-TE7 $\times$ 11	-3.206	2.190	10629
LE $\times$ 9-TE8 $\times$ 11	-3.248	2.189	11655
LE $\times$ 5-TE4 $\times$ 15	-1.493	2.152	6075
LE $\times$ 5-TE5 $\times$ 15	-1.725	2.168	6975
LE $\times$ 5-TE6 $\times$ 15	-2.530	2.195	8025
LE $\times$ 5-TE7 $\times$ 15	-2.786	2.197	9225
LE $\times$ 5-TE8 $\times$ 15	-2.938	2.199	10575

$t, \frac{b}{2}, \frac{h}{2} - t$ ) are reported in Table 1. To verify the proposed models, results attained with an ABAQUS 3D model are also listed, which uses uniformly meshed second-order brick elements (C3D20R). In the 3D model, five layers of elements are used through the thickness of each wall, and two hundred of elements are employed along the longitudinal direction.

Fig. 8 presents the contour plot of  $w$ , which also shows that the deformation only occurs in a limited area. By observing results in Table 1, it can be found that FE beam models with uniform LE and node-dependent TE/LE approximations lead to reasonable results with much fewer degrees of freedom, whereas Taylor-based models give erroneous evaluation especially in low-order cases. Models employing Taylor series show poor convergence with the increase of the polynomial order, which demonstrates that such models are less efficient compared with Lagrange-type kinematics in capturing the responses of thin-walled beams with open sections. With the FE beam models adopting variable TE/LE descriptions based on node-dependent kinematics, evaluation of  $w$  and  $\sigma_{yy}$  reach the desired accuracy gradually with the increase of order of Taylor-based cross-section functions, and stress  $\sigma_{yy}$  reaches convergence faster. Fig. 9 presents the variation of  $w$  and  $\sigma_{yy}$  along edge  $(a, y, h - t)$  obtained with different FE models.

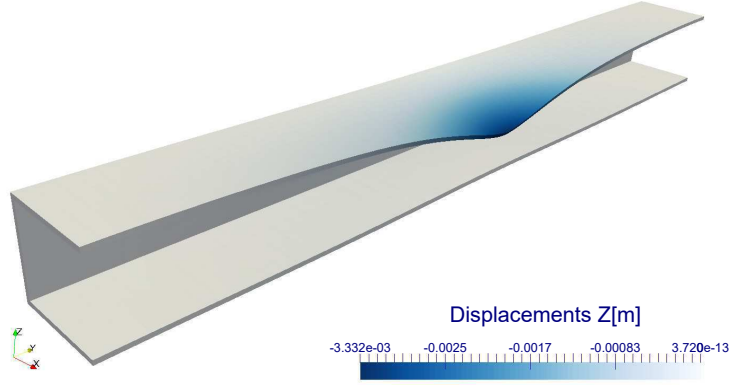


Figure 8: Contour plot of displacement of the beam with C-shaped section, obtained with uniform LE kinematics.

Table 2: Properties of the materials used in the eight-layered cantilever beam.

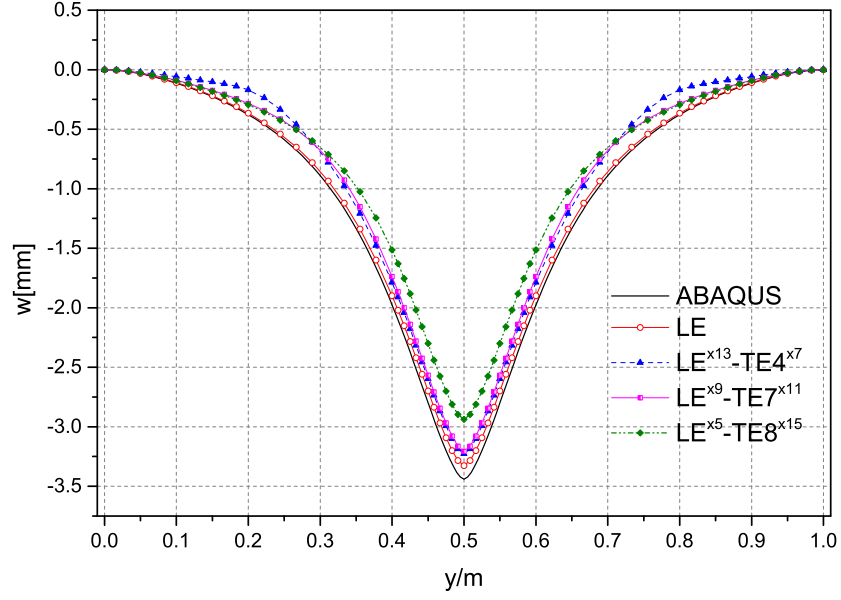
	$E_L$ [GPa]	$E_T$ [GPa]	$\nu_{LT}$	$G_{LT}$ [GPa]
Material-1	30	1	0.25	0.5
Material-2	5	1	0.25	0.5

Since TE models fail to give reasonable evaluation, the corresponding results are not plotted. It can be observed that, the distribution of  $w$  obtained with different models agree well with each other, and the variation is continuous. Meanwhile, for  $\sigma_{yy}$ , in the region out of the transition zone, a good estimation can be achieved. It should be noted that, along the axis of the beam, within the elements where different kinematics are used,  $\sigma_{yy}$  shows some oscillations, but accurate evaluation of  $\sigma_{yy}$  can still be achieved in the critical region. The oscillations of stresses in the bridging zone could be reduced by a gradual kinematic transition from refined model to lower-order theories. Whereas considering that the transition will be assigned to the area of less interest, such efforts are not necessary.

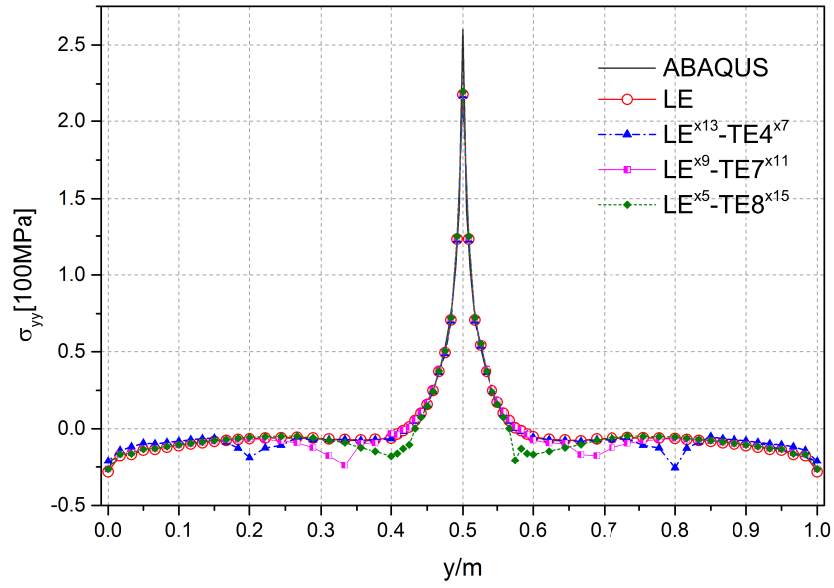
Fig. 10 shows the trend of the error (compared with full LE model) with the increases of the number of degrees of freedom used in FE models. It is obvious that node-dependent TE and LE kinematics reach a compromise between computational costs and accuracy, especially for stress  $\sigma_{yy}$  in the local region. With node-dependent kinematics, mixed TE/LE model reduced the error of  $\sigma_{yy}$  to a value lower than 2.0%. If the transition zone is properly selected (as in  $LE^{\times 13}$ - $TE^{n \times 7}$ ), with the increase of the expansion order in the outer and transition region, the error in the stress evaluation can be further reduced. From an engineering point of view,  $LE^{\times 13}$ - $TE^{2 \times 7}$  and  $LE^{\times 9}$ - $TE^{3 \times 11}$  can already give satisfactory stress evaluation.  $LE^{\times 5}$ - $TE^{2 \times 15}$  models lead to less accurate estimations, which demonstrates that the transition zone should be chosen considerably to guarantee the solution accuracy. Generally area with comparatively low stress gradients is appropriate, and in some situations numerical trials are necessary.

## 5.2 An eight-layered cantilever composite beam

In this section an eight-layers laminated cantilever beam is considered. The geometry and stacking sequence of the structure are shown in Fig. 11. The beam is loaded by an concentrated load of  $P = 0.2N$  at the central point of the free end, and clamped at the other end. The material properties are listed in Table 2. The axial direction of the two types of layers are along the longitudinal direction of the beam ( $y$  direction in Fig. 11).

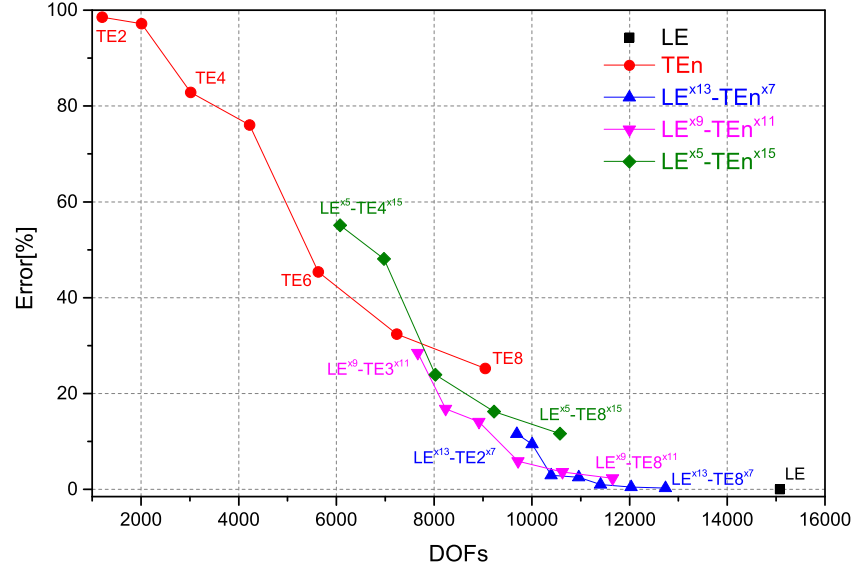


(a) Vertical displacement,  $w$ .

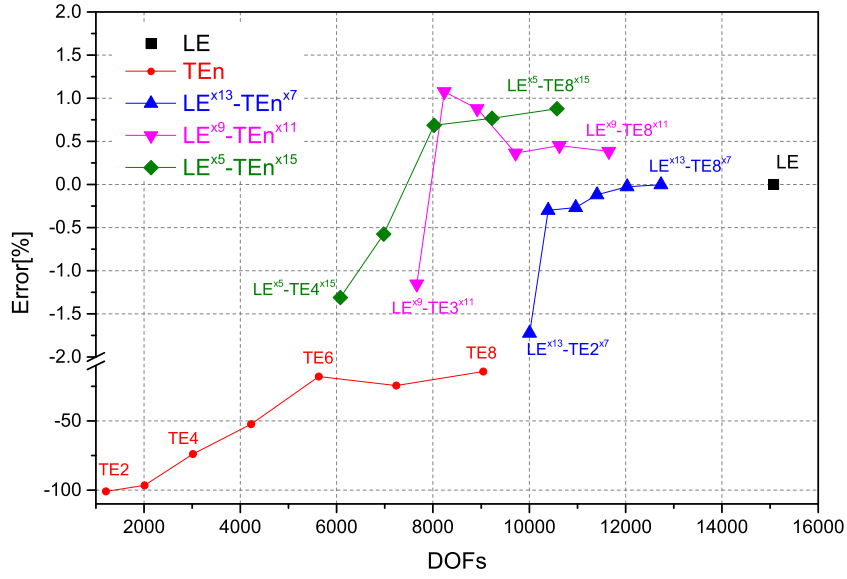


(b) Axial stress,  $\sigma_{yy}$ .

Figure 9: Variation of  $w$  and  $\sigma_{yy}$  along edge  $(a, y, h - t)$  on the beam with C-shaped section.



(a)  $w$



(b)  $\sigma_{yy}$

Figure 10: Relative error estimation of  $w$  and  $\sigma_{yy}$  on point  $B(a, \frac{b}{2}, h-t)$  on the beam with C-shaped section.

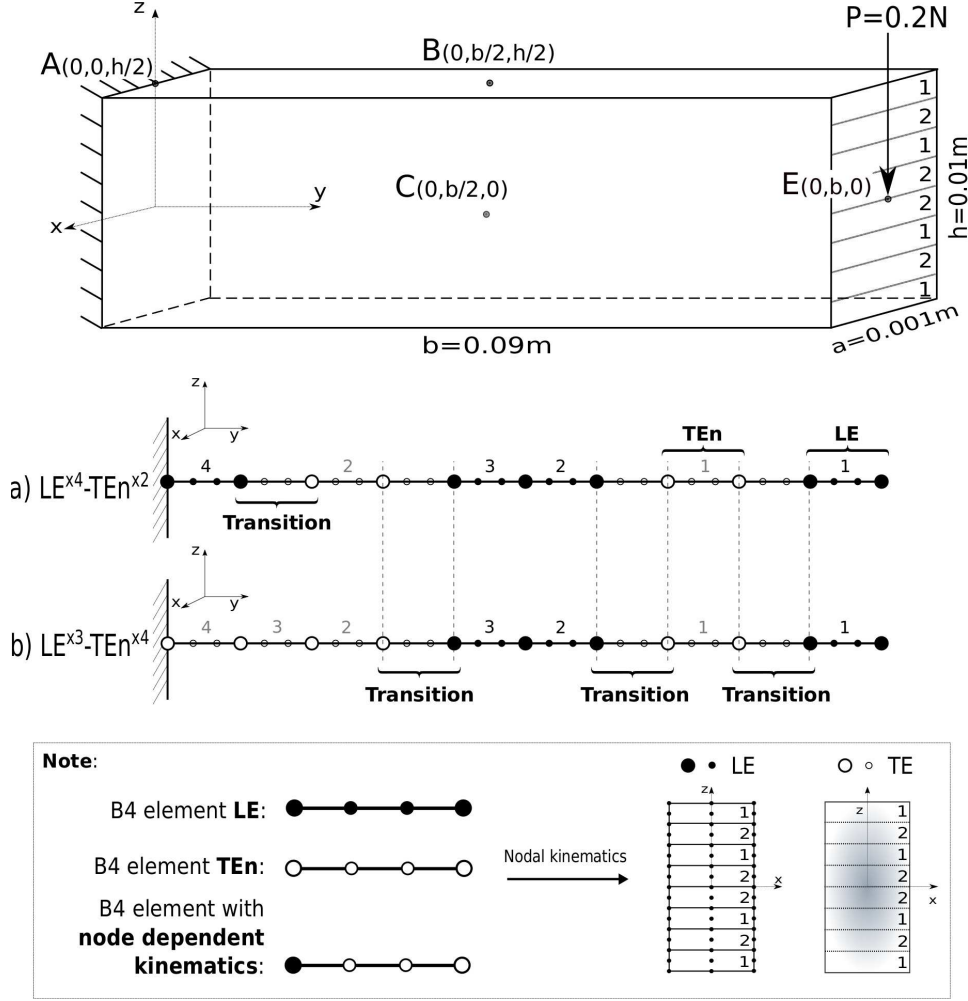


Figure 11: Geometry and FE modeling of the eight-layered cantilever beam.

For the convenience of comparison with results reported by various authors [54, 55, 56, 57], in this work the stress  $\sigma_{yy}$  is reported on point  $B(0, \frac{b}{2}, \frac{h}{2})$ ,  $\sigma_{yz}$  on point  $C(0, \frac{b}{2}, 0)$ , and  $w$  on  $E(0, b, 0)$ . At the same time, since stress concentration exists at the clamped and loading ends,  $\sigma_{yy}$  is reported also at point  $A(0, 0, \frac{h}{2})$ .

In FE models, the structure is discretized into ten B4 elements with node-dependent kinematics. Since the regions of interest are the two ends and the center of the beam, LE kinematics are applied to these regions, as demonstrated in Fig. 11. The case *a* adopts four elements with full LE description, and two elements completely based on TE kinematics, a)  $LE^4-TE^2$ . For comparison purposes, FE model b)  $LE^3-TE^4$  is also adopted. The B4 elements with variable kinematic are annotated in Fig. 11 together with the nodal kinematic descriptions. By observing results summarized in Table 3, it can be found that in this case, both LE and TE models can give good approximations. Differently from the thin-walled beam case discussed above, LE kinematics do not have obvious advantage over TE model considering both the accuracy and computational costs, and TE5 can lead to results with satisfactory accuracy.

Considering the through-the-thickness distribution of  $\sigma_{yy}$  and  $\sigma_{yz}$  at  $(0, \frac{b}{2}, \bar{z})$  shown in Fig. 12, it can be seen that an accurate description of  $\sigma_{yy}$  can be achieved with all the models considered. Otherwise, when the distribution of  $\sigma_{yz}$  is considered, the use of LE models is mandatory to obtain an accurate stress distribution. In this last case the use of the variable kinematic models could lead to a reduction of



Table 3: Displacement and stress evaluation of the eight-layered cantilever beam.

Model	$\sigma_{yy}$ [MPa] $A(0, 0, \frac{h}{2})$	$\sigma_{yy} \times 10^3$ [MPa] $B(0, \frac{b}{2}, \frac{h}{2})$	$\sigma_{yz} \times 10^2$ [MPa] $C(0, \frac{b}{2}, 0)$	$w \times 10^{-2}$ [mm] $E(0, b, 0)$	DOFs
Surana and Nguyen [54]		720		-3.03	
Carrera <i>et al.</i> [58]		730	-2.79	-3.05	4743
LE	1.689	729.6	-2.794	-3.049	4743
TE2	1.460	729.6	-1.999	-2.985	588
TE3	1.597	729.6	-2.822	-3.029	930
TE4	1.597	729.6	-2.822	-3.033	1395
TE5	1.671	729.7	-2.750	-3.034	1953
LE <sup>×4</sup> -TE2 <sup>×2</sup>	1.663	737.1	-2.482	-3.016	2583
LE <sup>×4</sup> -TE3 <sup>×2</sup>	1.689	730.9	-2.799	-3.048	2775
LE <sup>×4</sup> -TE4 <sup>×2</sup>	1.689	730.9	-2.799	-3.048	3015
LE <sup>×3</sup> -TE2 <sup>×4</sup>	1.460	737.1	-2.482	-3.014	2043
LE <sup>×3</sup> -TE3 <sup>×4</sup>	1.597	730.9	-2.799	-3.047	2283
LE <sup>×3</sup> -TE4 <sup>×4</sup>	1.597	730.9	-2.799	-3.047	2583

Table 4: Properties of the material used in the single-cell box beam.

$E_L$	$E_T, E_Z$	$\nu_{LT}, \nu_{LZ}, \nu_{TZ}$	$G_{LT}, G_{LZ}, G_{TZ}$
69.0 GPa	10.0 GPa	0.25	6.0 GPa

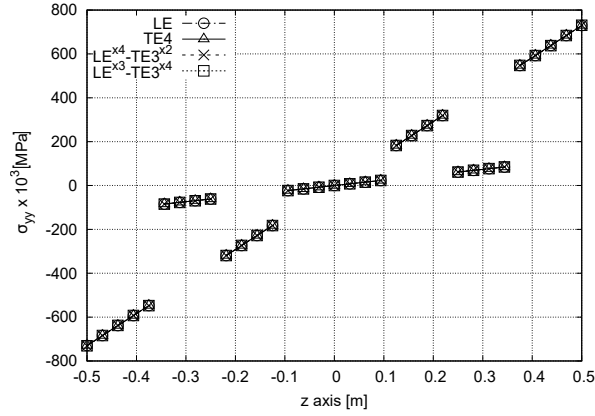
the computational cost maintaining a detailed result. Model LE<sup>×3</sup>-TE3<sup>×4</sup> is able to properly describe the stress field using less than 50% of the DOFs required by the LE model.

It can be found that FE models with node-dependent TE and LE kinematics can reach a balance between TE and LE models regarding the accuracy and computation costs. LE<sup>×4</sup>-TE3<sup>×2</sup> and LE<sup>×3</sup>-TE3<sup>×4</sup> can reduce the number of degrees of freedom to a great extent while guaranteeing the accuracy. Results also show that if stress at the clamped end is not of interest, a lower order model can be used in this part of the structure without affecting the accuracy of results where an higher-order model is required.

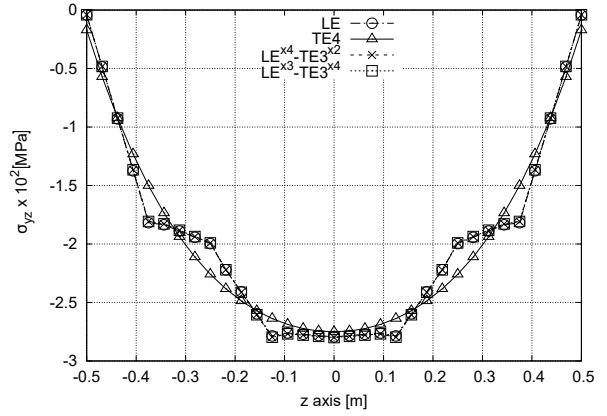
### 5.3 A composite single-cell box beam

In this section a thin-walled composite beam with a cross-section in the shape of a single-cell box is considered. The structure is clamped at one end and loaded with two vertical concentrated loads in the upper corners on the other end, as shown in Fig. 15.

The dimensions of the beam are: length  $L=242$  mm, height  $h=13.6$  mm, width  $a=24.2$  mm and thickness  $t=0.762$  mm. Fig. 15 shows the cross-sectional geometry. The thin-walled beam is built with a composite material which has the properties reported in Table 4. Two different laminations have been used:  $[0^\circ/90^\circ]$  lay-up for the webs and  $[45^\circ/+45^\circ]$  lay-up for the flanges. Results obtained using different models have been considered and compared. Fig. 15 show the cross-sectional discretization used when an LE approximation is used. Fig. 15a shows a model which uses 16 L9 elements while, in Fig. 15b, is reported a more refined model created with 24 L9 elements. Ten B4 elements have been used along the beam axis. Results have been compared with those from literature, see [58], obtained with refined one-dimensional models with constant nodal kinematics. Moreover, a refined solid model



(a)  $\sigma_{yy}$  at  $(0, \frac{b}{2}, \bar{z})$



(b)  $\sigma_{yz}$  at  $(0, \frac{b}{2}, \bar{z})$

Figure 12: Plots of stresses distribution obtained with different models for the eight-layered cantilever beam.

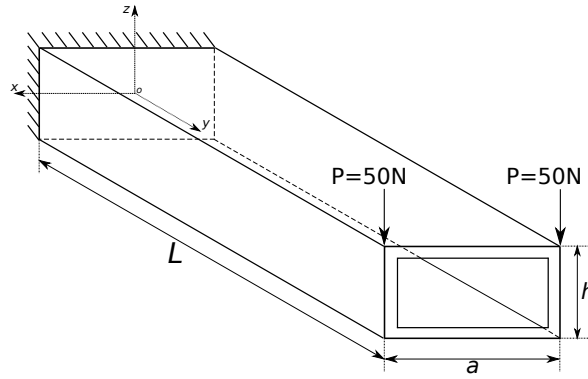


Figure 13: Geometry feature and loading of the thin-walled composite beam.

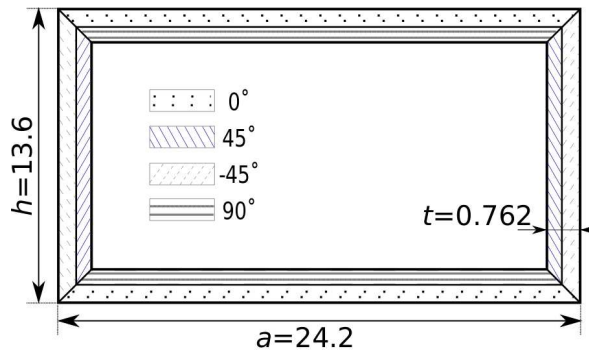


Figure 14: Layup of the cross-section of the single-cell box beam.

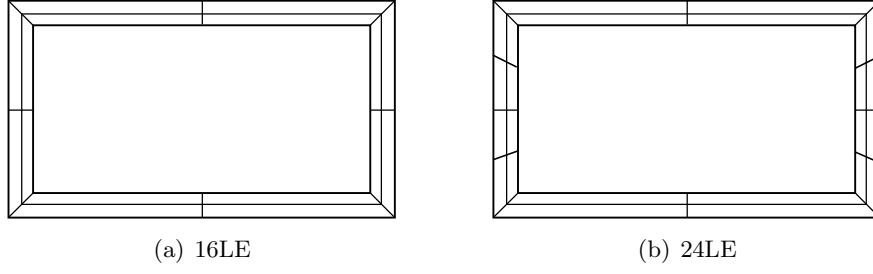


Figure 15: Domain discretization of the cross-section of the single-cell box beam.

Table 5: Displacement and stress evaluation of the single-cell composite beam.

Model	$-u_z[\text{mm}]$ (0, $L$ , $h/2$ )	$\sigma_{yy}[\text{MPa}]$ (0, $L/2$ , $h/2$ )	$\sigma_{yy}[\text{MPa}]$ (0, 0, $h/2$ )	$\sigma_{yz}[\text{MPa}]$ ( $b/2$ , $L/2$ , $h/4$ )	DOFs
ABAQUS-3D	7.199	85.086	161.205	-8.413	326160
Carrera <i>et al.</i> [58]	7.16	85.30	165.77	-8.94	2604
TE2	7.044	84.50	166.7	-8.895	558
TE3	7.094	84.64	163.8	-9.705	930
TE4	7.126	85.73	166.4	-7.950	1395
TE5	7.162	85.47	166.9	-8.105	1953
TE6	7.159	85.14	163.6	-7.945	2604
TE7	7.157	85.42	159.5	-8.239	3348
TE8	7.150	85.29	163.4	-9.155	4185
TE9	7.159	85.75	161.8	-8.411	5115
TE10	7.157	85.963	161.571	-8.314	6138
16L9	7.123	85.615	165.827	-7.445	7440
24L9	7.123	85.797	167.116	-10.975	11160
TE3/TE6	7.140	84.949	163.678	-8.326	1686
TE3/16L9	7.138	85.112	163.809	-7.363	3660

has been developed using the commercial code ABAQUS.

Table 5 shows results obtained using different structural models. The displacement evaluated at the free tip, point (0,  $L$ ,  $h/2$ ), has been reported in the second column. Columns three to four report the normal stress and at the mid-span, point (0,  $L/2$ ,  $h/2$ ), and at the root, point (0, 0,  $h/2$ ). Column five shows the shear stress at the mid-span, point ( $b/2$ ,  $L/2$ ,  $h/4$ ), while the last column reports the number of DOFs. At first TE models with order form 2 to 10 have been considered. Results show that models with order higher than 5 are able to provide excellent results in terms of stresses and displacements. Some oscillation can still be seen in the shear stress. Results obtained with these models can be successfully compared with those from the solid model. Two LE models have also been considered; the first has 16 L9 elements on the cross-section while the second uses 24 L9 elements. These models provide accurate results but the computational costs are much higher than those of the TE models. Two node-dependent kinematic models have been introduced to reduce the computational costs preserving the same accuracy. Both the models use the lower-order model at the beam ends, in particular at the first and the last three elements. The higher order model is used in the four central elements, where results are evaluated. Results obtained using these models are reported in the last two rows of Table 5.

Table 6: Degrees of freedom, nonzeros of the stiffness matrix and solution times for different models.

Model	DOFs	Nonzeros $\times 10^3$	Solution time [s]
TE2	558	49	0.01
TE3	930	136	0.03
TE4	1395	306	0.08
TE5	1953	599	0.14
TE6	2604	1065	0.26
TE7	3348	1761	0.43
TE8	4185	2752	0.68
TE9	5115	4111	1.05
TE10	6138	5919	1.81
16L9	7440	1477	0.35
24L9	11160	2217	0.51
TE3/TE6	1686	531	0.13
TE3/16L9	3660	753	0.22

Table 6 reports some details about the computational costs. The number of degrees of freedom is compared with the nonzeros of the stiffness matrix and the solution times. The results show that, even if LE models have a high number of DOFs, they provide a more sparse matrix, that is the solution times are lower with respect a TE models with the same number of DOFs. Otherwise, low order TE models are still more convenient than LE models, that is, the node-dependent approach provide a good compromise between the low computational cost of the low-order TE models and the high accuracy of the LE models.

Fig. 16 shows the shear stress distribution through the flange thickness. Results show that the mixed model TE3/TE6 is able to describe the stress distribution accurately. Even if the TE3 model is cheaper than the other models considered, it is not able to provide accurate results. TE8 and 16L9 also produce accurate results but they require a higher number of DOFs with respect to the TE3/TE6 model.

Fig. 17 and Fig. 18 show the shear stress distribution through the outer and inner layers of the flange. As observed in the previous figure, also in this case the use of a node-dependent kinematics allows accurate results to be obtained with a lower computational cost.

## 6 Conclusions

Through the introduction of cross-section functions into refined beam models, and further defining cross-section function upon specific nodes, Carrera Unified Formulation (CUF) makes it convenient to develop node-dependent kinematic models, in which the kinematic description can be different from node to node. Through Lagrangian nodal shape functions, node-dependent cross-section functions are interpolated on the axial domain to construct an advanced beam element. FE models with variable ESL/LW kinematic capabilities can be constructed without using any *ad hoc* assumptions, which can reduce the computational efforts without losing accuracy. These types of FE models are appropriate to be employed in the analysis of composite structures with local effects to be captured.

In this paper, FE models with node-dependent kinematics are used in three numerical cases, including both isotropic and composite laminated structures, both classical and thin-walled beams. Based on the above assessments, the following conclusions can be drawn:

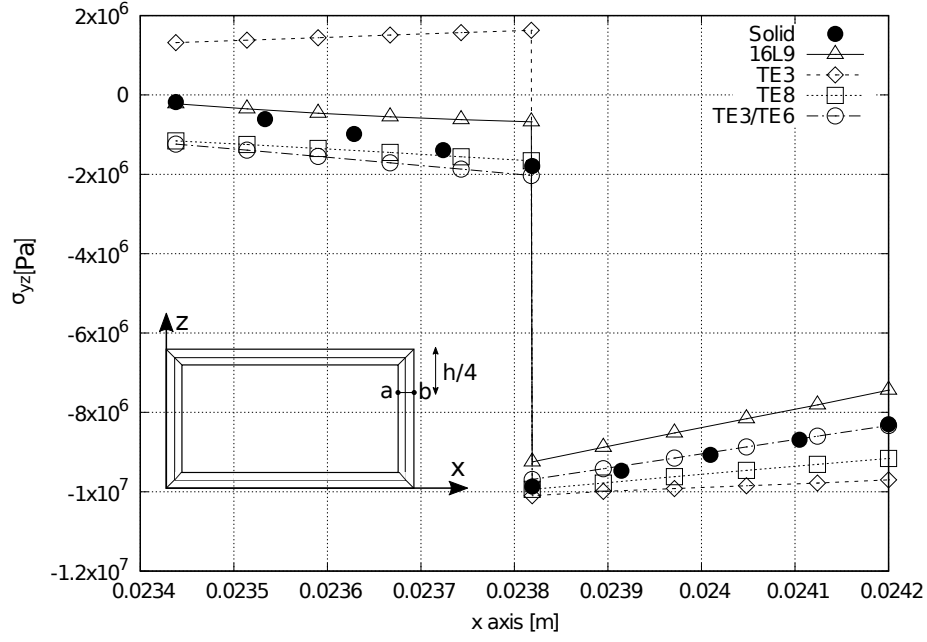


Figure 16: Shear stress distribution through the flange thickness. Stresses are evaluated over the path  $a - b$ , on the mid-span section on the single-cell box beam.

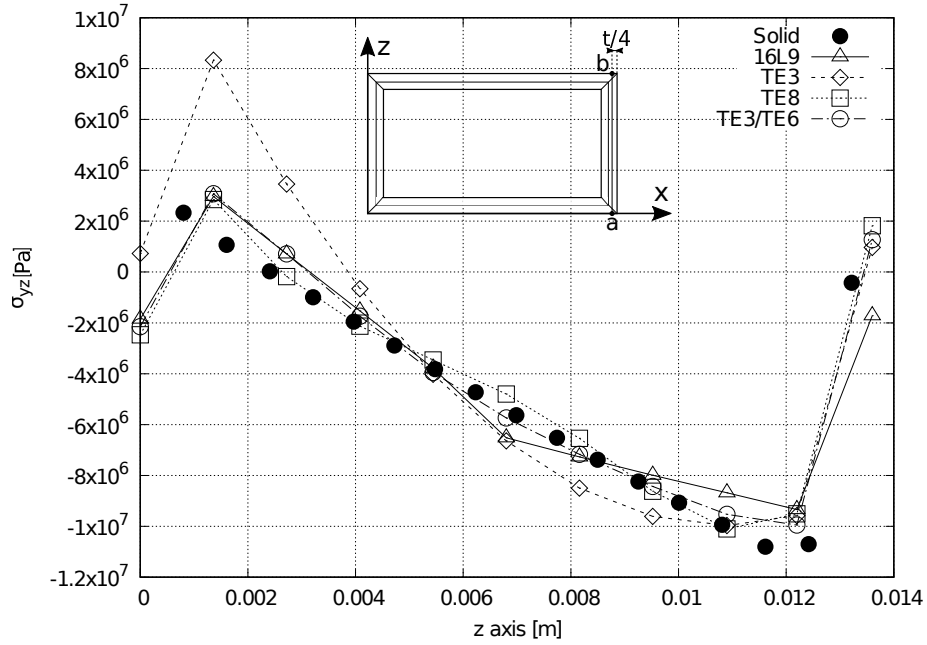


Figure 17: Shear stress distribution through the outer layer of the flange. Stresses are evaluated over the path  $a - b$ , on the mid-span section on the single-cell box beam.

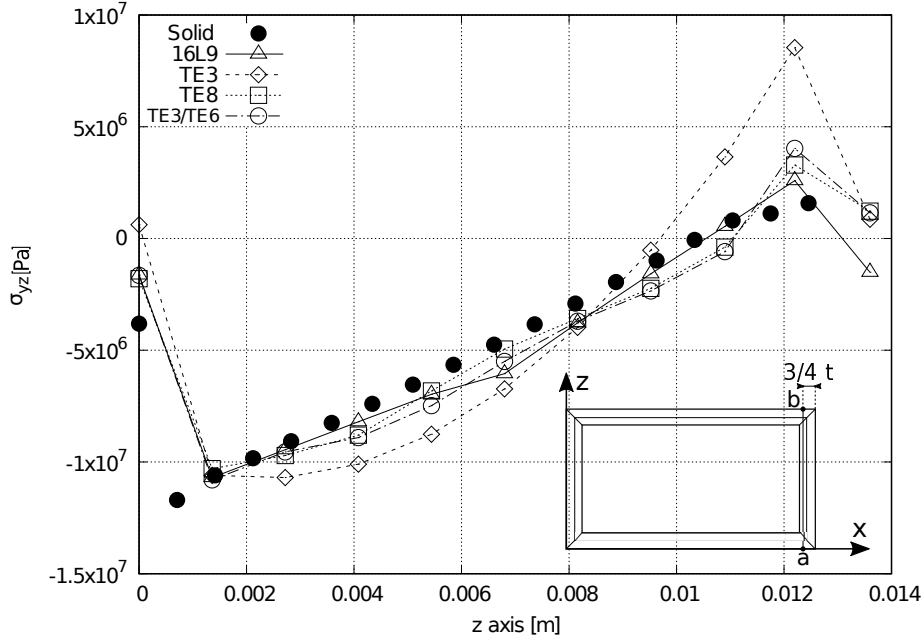


Figure 18: Shear stress distribution through the inner layer of the flange. Stresses are evaluated over the path  $a - b$ , on the mid-span section on the single-cell box beam.

- Node-dependent kinematics provide a solution to integrate the accuracy of the LE models and the low computational cost of the TE models to obtain optimal beam models in a natural way.
- When used to bridge a locally refined model with LE to a global model with lower-order kinematics, such beam models can reduce the computational costs of FE analysis while guaranteeing the approximation accuracy.
- Such an approach can guarantee the continuity of the displacement field in the bridging zone naturally without using special coupling methods, leading to compact FE formulations for the analysis of structures with local effects to be addressed.
- The use of the Carrera Unified Formulation allows the formulation of the node-dependent kinematic models to be derived in a general form able to deal with any cross-sectional kinematic assumption.
- When used in global-local analysis, the proposed approach adopts only one set of FE mesh, and the local region will be approximated by adopting refined nodal kinematics.

In a word, as an innovative and versatile approach, node-dependent kinematics can act as a new method to be applied to build more efficient FE models in global-local analysis.

## 7 Acknowledgment

This research work has been carried out within the project FULLCOMP (FULLy analysis, design, manufacturing, and health monitoring of COMposite structures), funded by the European Union Horizon 2020 Research and Innovation program under the Marie Skłodowska Curie grant agreement No. 642121.

## 8 Appendix: Fundamental nucleus for node-dependent kinematic 1D FE models

The fundamental nucleus in the case of node-dependent kinematic and orthotropic material can be written in the following form:

$$\begin{aligned}
K_{xx}^k &= \tilde{C}_{11}^k I_{ij} E_{\tau, xs, x}^{ij(k)} + \tilde{C}_{15}^k I_{ij} E_{\tau, zs, x}^{ij(k)} + \tilde{C}_{15}^k I_{ij} E_{\tau, xs, z}^{ij(k)} + \\
&\quad \tilde{C}_{16}^k I_{ij, y} E_{\tau, xs}^{ij(k)} + \tilde{C}_{16}^k I_{i, yj} E_{\tau s, x}^{ij(k)} + \tilde{C}_{55}^k I_{ij} E_{\tau, zs, z}^{ij(k)} + \\
&\quad \tilde{C}_{56}^k I_{ij, y} E_{\tau, zs}^{ij(k)} + \tilde{C}_{56}^k I_{i, yj} E_{\tau s, z}^{ij(k)} + \tilde{C}_{66}^k I_{i, yj, y} E_{\tau s}^{ij(k)} \\
K_{xy}^k &= \tilde{C}_{12}^k I_{i, yj} E_{\tau s, x}^{ij(k)} + \tilde{C}_{14}^k I_{ij} E_{\tau, zs, x}^{ij(k)} + \tilde{C}_{16}^k I_{ij} E_{\tau, xs, x}^{ij(k)} + \\
&\quad \tilde{C}_{25}^k I_{i, yj} E_{\tau s, z}^{ij(k)} + \tilde{C}_{26}^k I_{i, yj, y} E_{\tau s}^{ij(k)} + \tilde{C}_{45}^k I_{ij} E_{\tau, zs, z}^{ij(k)} + \\
&\quad \tilde{C}_{46}^k I_{ij, y} E_{\tau, zs}^{ij(k)} + \tilde{C}_{56}^k I_{ij} E_{\tau, xs, z}^{ij(k)} + \tilde{C}_{66}^k I_{ij, y} E_{\tau, xs}^{ij(k)} \\
K_{xz}^k &= \tilde{C}_{13}^k I_{ij} E_{\tau, zs, x}^{ij(k)} + \tilde{C}_{14}^k I_{i, yj} E_{\tau s, x}^{ij(k)} + \tilde{C}_{15}^k I_{ij} E_{\tau, xs, x}^{ij(k)} + \\
&\quad \tilde{C}_{35}^k I_{ij} E_{\tau, zs, z}^{ij(k)} + \tilde{C}_{36}^k I_{ij, y} E_{\tau, zs}^{ij(k)} + \tilde{C}_{45}^k I_{i, yj} E_{\tau s, z}^{ij(k)} + \\
&\quad \tilde{C}_{46}^k I_{i, yj, y} E_{\tau s}^{ij(k)} + \tilde{C}_{55}^k I_{ij} E_{\tau, xs, z}^{ij(k)} + \tilde{C}_{56}^k I_{ij, y} E_{\tau, xs}^{ij(k)} \\
K_{yx}^k &= \tilde{C}_{12}^k I_{ij, y} E_{\tau, xs}^{ij(k)} + \tilde{C}_{14}^k I_{ij} E_{\tau, xs, z}^{ij(k)} + \tilde{C}_{16}^k I_{ij} E_{\tau, xs, x}^{ij(k)} + \\
&\quad \tilde{C}_{25}^k I_{ij, y} E_{\tau, zs}^{ij(k)} + \tilde{C}_{26}^k I_{i, yj, y} E_{\tau s}^{ij(k)} + \tilde{C}_{45}^k I_{ij} E_{\tau, zs, z}^{ij(k)} + \\
&\quad \tilde{C}_{46}^k I_{i, yj} E_{\tau s, z}^{ij(k)} + \tilde{C}_{56}^k I_{ij} E_{\tau, zs, x}^{ij(k)} + \tilde{C}_{66}^k I_{i, yj} E_{\tau s, x}^{ij(k)} \\
K_{yy}^k &= \tilde{C}_{22}^k I_{i, yj, y} E_{\tau s}^{ij(k)} + \tilde{C}_{24}^k I_{ij, y} E_{\tau, zs}^{ij(k)} + \tilde{C}_{24}^k I_{i, yj} E_{\tau s, z}^{ij(k)} + \\
&\quad \tilde{C}_{26}^k I_{ij, y} E_{\tau, xs}^{ij(k)} + \tilde{C}_{26}^k I_{i, yj} E_{\tau s, x}^{ij(k)} + \tilde{C}_{44}^k I_{ij} E_{\tau, zs, z}^{ij(k)} + \\
&\quad \tilde{C}_{46}^k I_{ij} E_{\tau, zs, x}^{ij(k)} + \tilde{C}_{46}^k I_{ij} E_{\tau, xs, z}^{ij(k)} + \tilde{C}_{66}^k I_{ij} E_{\tau, xs, x}^{ij(k)} \\
K_{yz}^k &= \tilde{C}_{23}^k I_{ij, y} E_{\tau, zs}^{ij(k)} + \tilde{C}_{24}^k I_{i, yj, y} E_{\tau s}^{ij(k)} + \tilde{C}_{25}^k I_{ij, y} E_{\tau, xs}^{ij(k)} + \\
&\quad \tilde{C}_{34}^k I_{ij} E_{\tau, zs, z}^{ij(k)} + \tilde{C}_{36}^k I_{ij} E_{\tau, zs, x}^{ij(k)} + \tilde{C}_{44}^k I_{i, yj} E_{\tau s, z}^{ij(k)} + \\
&\quad \tilde{C}_{45}^k I_{ij} E_{\tau, xs, z}^{ij(k)} + \tilde{C}_{46}^k I_{i, yj} E_{\tau s, x}^{ij(k)} + \tilde{C}_{56}^k I_{ij} E_{\tau, xs, x}^{ij(k)} \\
K_{zx}^k &= \tilde{C}_{13}^k I_{ij} E_{\tau, xs, z}^{ij(k)} + \tilde{C}_{14}^k I_{ij, y} E_{\tau, xs}^{ij(k)} + \tilde{C}_{15}^k I_{ij} E_{\tau, xs, x}^{ij(k)} + \\
&\quad \tilde{C}_{35}^k I_{ij} E_{\tau, zs, z}^{ij(k)} + \tilde{C}_{36}^k I_{i, yj} E_{\tau s, z}^{ij(k)} + \tilde{C}_{45}^k I_{ij, y} E_{\tau, zs}^{ij(k)} + \\
&\quad \tilde{C}_{46}^k I_{i, yj, y} E_{\tau s}^{ij(k)} + \tilde{C}_{55}^k I_{ij} E_{\tau, zs, x}^{ij(k)} + \tilde{C}_{56}^k I_{i, yj} E_{\tau s, x}^{ij(k)} \\
K_{zy}^k &= \tilde{C}_{23}^k I_{i, yj} E_{\tau s, z}^{ij(k)} + \tilde{C}_{24}^k I_{i, yj, y} E_{\tau s}^{ij(k)} + \tilde{C}_{25}^k I_{i, yj} E_{\tau s, x}^{ij(k)} + \\
&\quad \tilde{C}_{34}^k I_{ij} E_{\tau, zs, z}^{ij(k)} + \tilde{C}_{36}^k I_{ij} E_{\tau, xs, z}^{ij(k)} + \tilde{C}_{44}^k I_{ij, y} E_{\tau, zs}^{ij(k)} + \\
&\quad \tilde{C}_{45}^k I_{ij} E_{\tau, zs, x}^{ij(k)} + \tilde{C}_{46}^k I_{ij, y} E_{\tau, xs}^{ij(k)} + \tilde{C}_{56}^k I_{ij} E_{\tau, xs, x}^{ij(k)} \\
K_{zz}^k &= \tilde{C}_{33}^k I_{ij} E_{\tau, zs, z}^{ij(k)} + \tilde{C}_{34}^k I_{ij, y} E_{\tau, zs}^{ij(k)} + \tilde{C}_{34}^k I_{i, yj} E_{\tau s, z}^{ij(k)} + \\
&\quad \tilde{C}_{35}^k I_{ij} E_{\tau, zs, x}^{ij(k)} + \tilde{C}_{35}^k I_{ij} E_{\tau, xs, z}^{ij(k)} + \tilde{C}_{44}^k I_{i, yj, y} E_{\tau s}^{ij(k)} + \\
&\quad \tilde{C}_{45}^k I_{ij, y} E_{\tau, xs}^{ij(k)} + \tilde{C}_{45}^k I_{i, yj} E_{\tau s, x}^{ij(k)} + \tilde{C}_{55}^k I_{ij} E_{\tau, xs, x}^{ij(k)}
\end{aligned} \tag{20}$$

The integrals of the product of the cross-section functions defined on the transverse domain  $\Omega$  or

the thickness domain of a layer  $\Omega^k$  are defined as:

$$\begin{aligned}
E_{\tau s}^{ij(k)} &= \int_{\Omega(k)} F_{\tau}^{i(k)} F_s^{j(k)} dx dz, & E_{\tau, x s}^{ij(k)} &= \int_{\Omega(k)} F_{\tau, x}^{i(k)} F_s^{j(k)} dx dz, & E_{\tau s, x}^{ij(k)} &= \int_{\Omega(k)} F_{\tau}^{i(k)} F_{s, x}^{j(k)} dx dz, \\
E_{\tau, z s}^{ij(k)} &= \int_{\Omega(k)} F_{\tau, z}^{i(k)} F_s^{j(k)} dx dz, & E_{\tau s, z}^{ij(k)} &= \int_{\Omega(k)} F_{\tau}^{i(k)} F_{s, z}^{j(k)} dx dz, & E_{\tau, x s, x}^{ij(k)} &= \int_{\Omega(k)} F_{\tau, x}^{i(k)} F_{s, x}^{j(k)} dx dz, \\
E_{\tau, z s, z}^{ij(k)} &= \int_{\Omega(k)} F_{\tau, z}^{i(k)} F_{s, z}^{j(k)} dx dz, & E_{\tau, x s, z}^{ij(k)} &= \int_{\Omega(k)} F_{\tau, x}^{i(k)} F_{s, z}^{j(k)} dx dz, & E_{\tau, z s, x}^{ij(k)} &= \int_{\Omega(k)} F_{\tau, z}^{i(k)} F_{s, x}^{j(k)} dx dz.
\end{aligned} \tag{21}$$

and the integrals of the nodal shape functions along  $y$  over the axial domain  $L$  of a beam element are denoted as:

$$\begin{aligned}
I_{ij} &= \int_L N_i N_j dy, & I_{i, y} &= \int_L N_i N_{j, y} dy, \\
I_{i, y j} &= \int_L N_{i, y} N_j dy, & I_{i, y j, y} &= \int_L N_{i, y} N_{j, y} dy,
\end{aligned} \tag{22}$$

## References

- [1] S. Timoshenko, On the correction for shear of the differential equation for transverse vibrations of bar for uniform cross-section, *Philosophical Magazine Series 6* 41 (245) (1921) 744–746.
- [2] V. Z. Vlasov, *Thin-walled elastic beams*, National Technical Information Service, 1984.
- [3] P. Friberg, Beam element matrices derived from vlasov's theory of open thin-walled elastic beams, *International Journal for Numerical Methods in Engineering* 21 (7) (1985) 1205–1228.
- [4] R. D. Ambrosini, J. D. Riera, R. F. Danesi, A modified vlasov theory for dynamic analysis of thin-walled and variable open section beams, *Engineering Structures* 22 (8) (2000) 890–900.
- [5] I. Mechab, N. E. Meiche, F. Bernard, Analytical study for the development of a new warping function for high order beam theory, *Composites Part B: Engineering* 119 (2017) 18 – 31. doi:<https://doi.org/10.1016/j.compositesb.2017.03.006>.
- [6] N.-I. Kim, J. Lee, Exact solutions for coupled responses of thin-walled fg sandwich beams with non-symmetric cross-sections, *Composites Part B: Engineering* 122 (2017) 121 – 135. doi:<https://doi.org/10.1016/j.compositesb.2017.04.016>.
- [7] R. Schardt, Eine erweiterung der technischen biegetheorie zur berechnung prismatischer faltwerke, *Der Stahlbau* 35 (1966) 161–171.
- [8] J. Davies, P. Leach, First-order generalised beam theory, *Journal of Constructional Steel Research* 31 (2-3) (1994) 187–220.
- [9] J. Davies, P. Leach, D. Heinz, Second-order generalised beam theory, *Journal of Constructional Steel Research* 31 (2) (1994) 221–241.
- [10] N. Silvestre, D. Camotim, First-order generalised beam theory for arbitrary orthotropic materials, *Thin-Walled Structures* 40 (9) (2002) 755–789.
- [11] V. Berdichevskii, Equations of the theory of anisotropic inhomogeneous rods, in: *Soviet Physics Doklady*, Vol. 21, 1976, p. 286.



- [12] V. Giavotto, M. Borri, P. Mantegazza, G. Ghiringhelli, V. Carmaschi, G. Maffioli, F. Mussi, Anisotropic beam theory and applications, *Computers & Structures* 16 (1-4) (1983) 403–413.
- [13] V. V. Volovoi, D. H. Hodges, V. L. Berdichevsky, V. G. Sutyrin, Asymptotic theory for static behavior of elastic anisotropic I-beams, *International Journal of Solids and Structures* 36 (7) (1999) 1017–1043.
- [14] W. Yu, V. V. Volovoi, D. H. Hodges, X. Hong, Validation of the variational asymptotic beam sectional analysis, *AIAA Journal* 40 (10) (2002) 2105–2112.
- [15] W. Yu, D. H. Hodges, Asymptotic approach for thermoelastic analysis of laminated composite plates, *Journal of Engineering Mechanics* 130 (5) (2004) 531–540.
- [16] E. Carrera, Theories and finite elements for multilayered, anisotropic, composite plates and shells, *Archives of Computational Methods in Engineering* 9 (2) (2002) 87–140.
- [17] E. Carrera, G. Giunta, M. Petrolo, *Beam structures: classical and advanced theories*, John Wiley & Sons, 2011.
- [18] E. Carrera, M. Petrolo, E. Zappino, Performance of cuf approach to analyze the structural behavior of slender bodies, *Journal of Structural Engineering* 138 (2) (2011) 285–297.
- [19] E. Carrera, M. Filippi, E. Zappino, Free vibration analysis of laminated beam by polynomial, trigonometric, exponential and zig-zag theories, *Journal of Composite Materials* (2013) 0021998313497775.
- [20] M. Cinefra, S. Valvano, E. Carrera, Heat conduction and thermal stress analysis of laminated composites by a variable kinematic mitc9 shell element, *Curved and Layered Structures* 2 (1).
- [21] M. Cinefra, S. Valvano, A variable kinematic doubly-curved MITC9 shell element for the analysis of laminated composites, *Mechanics of Advanced Materials and Structures* 23 (11) (2016) 1312–1325.
- [22] A. Airoidi, A. Baldi, P. Bettini, G. Sala, Efficient modelling of forces and local strain evolution during delamination of composite laminates, *Composites Part B: Engineering* 72 (2015) 137 – 149.
- [23] S. G. Haryadi, R. K. Kapania, R. T. Haftka, Global/local analysis of composite plates with cracks, *Composites Part B: Engineering* 29 (3) (1998) 271–276.
- [24] T. Kubiak, Z. Kolakowski, J. Swiniarski, M. Urbaniak, A. Gliszczynski, Local buckling and post-buckling of composite channel-section beams numerical and experimental investigations, *Composites Part B: Engineering* 91 (2016) 176 – 188.
- [25] W. Prager, Variational principles of linear elastostatics for discontinuous displacements, strains and stresses, *Recent Progress in Applied Mechanics. The Folkey Odquist Volume*. Stockholm: Almqvist and Wiksell (1967) 463–474.
- [26] E. Carrera, A. Pagani, M. Petrolo, Use of lagrange multipliers to combine 1d variable kinematic finite elements, *Computers & Structures* 129 (2013) 194–206.
- [27] M. A. Aminpour, J. B. Ransom, S. L. McCleary, A coupled analysis method for structures with independently modelled finite element subdomains, *International Journal for Numerical Methods in Engineering* 38 (21) (1995) 3695–3718.
- [28] J. B. Ransom, On Multifunctional Collaborative Methods in Engineering Science, Tech. rep. (Sep. 2001).

- [29] F. Brezzi, L. D. Marini, The three-field formulation for elasticity problems, *GAMM-Mitteilungen* 28 (2) (2005) 124–153.
- [30] P. Blanco, R. Feijóo, S. Urquiza, A variational approach for coupling kinematically incompatible structural models, *Computer Methods in Applied Mechanics and Engineering* 197 (17) (2008) 1577–1602.
- [31] P. Blanco, P. Gervasio, A. Quarteroni, Extended variational formulation for heterogeneous partial differential equations, *Computational Methods in Applied Mathematics Comput. Methods Appl. Math.* 11 (2) (2011) 141–172.
- [32] C. Wenzel, P. Vidal, M. DOttavio, O. Polit, Coupling of heterogeneous kinematics and finite element approximations applied to composite beam structures, *Composite Structures* 116 (2014) 177–192.
- [33] J. Fish, L. Pan, V. Belsky, S. Goma, Unstructured multigrid method for shells, *International Journal for Numerical Methods in Engineering* 39 (7) (1996) 1181–1197.
- [34] J. Fish, The s-version of the finite element method, *Computers & Structures* 43 (3) (1992) 539–547.
- [35] J. W. Park, J. W. Hwang, Y. H. Kim, Efficient finite element analysis using mesh superposition technique, *Finite Elements in Analysis and Design* 39 (7) (2003) 619–638.
- [36] R. E. Bank, The efficient implementation of local mesh refinement algorithms, *Adaptive computational methods for partial differential equations* (1983) 74–81.
- [37] J. Reddy, D. Robbins, Theories and computational models for composite laminates, *Applied Mechanics Reviews* 47 (6) (1994) 147–169.
- [38] J. N. Reddy, *Mechanics of laminated composite plates and shells: theory and analysis*, CRC Press, 2004.
- [39] H. B. Dhia, Multiscale mechanical problems: the arlequin method, *Comptes Rendus de l’Academie des Sciences Series IIB Mechanics Physics Astronomy* 12 (326) (1998) 899–904.
- [40] H. B. Dhia, G. Rateau, The arlequin method as a flexible engineering design tool, *International Journal for Numerical Methods in Engineering* 62 (11) (2005) 1442–1462.
- [41] F. Biscani, G. Giunta, S. Belouettar, E. Carrera, H. Hu, Variable kinematic beam elements coupled via arlequin method, *Composite Structures* 93 (2) (2011) 697–708.
- [42] F. Biscani, G. Giunta, S. Belouettar, E. Carrera, H. Hu, Variable kinematic plate elements coupled via arlequin method, *International Journal for Numerical Methods in Engineering* 91 (12) (2012) 1264–1290.
- [43] F. Biscani, P. Nali, S. Belouettar, E. Carrera, Coupling of hierarchical piezoelectric plate finite elements via arlequin method, *Journal of Intelligent Material Systems and Structures* (2012) 1045389X12437885.
- [44] H. Hu, S. Belouettar, M. Potier-Ferry, et al., Multi-scale modelling of sandwich structures using the arlequin method part i: Linear modelling, *Finite Elements in Analysis and Design* 45 (1) (2008) 37–51.
- [45] H. Hu, S. Belouettar, M. Potier-Ferry, A. Makradi, et al., Multi-scale nonlinear modelling of sandwich structures using the Arlequin method, *Composite Structures* 92 (2) (2010) 515–522.

- [46] Q. He, H. Hu, S. Belouettar, G. Guinta, K. Yu, Y. Liu, F. Biscani, E. Carrera, M. Potier-Ferry, Multi-scale modelling of sandwich structures using hierarchical kinematics, *Composite Structures* 93 (9) (2011) 2375–2383.
- [47] E. Carrera, M. Cinefra, M. Petrolo, E. Zappino, *Finite element analysis of structures through unified formulation*, John Wiley & Sons, 2014.
- [48] E. Carrera, E. Zappino, Analysis of complex structures coupling variable kinematics one-dimensional models, in: *ASME 2014 International Mechanical Engineering Congress and Exposition*, American Society of Mechanical Engineers, 2014, pp. V001T01A023–V001T01A023.
- [49] E. Zappino, G. Li, A. Pagani, E. Carrera, Global-local analysis of laminated plates by node-dependent kinematic finite elements with variable ESL/LW capabilities, *Composite Structures*. In press. doi:doi.org/10.1016/j.compstruct.2017.03.057.
- [50] E. Carrera, A. Pagani, S. Valvano, Multilayered plate elements accounting for refined theories and node-dependent kinematics, *Composites Part B: Engineering* 114 (2017) 189–210.
- [51] M. B. Dehkordi, S. Khalili, E. Carrera, Non-linear transient dynamic analysis of sandwich plate with composite face-sheets embedded with shape memory alloy wires and flexible core-based on the mixed lw (layer-wise)/esl (equivalent single layer) models, *Composites Part B: Engineering* 87 (2016) 59–74.
- [52] E. Carrera, A. Pagani, S. Valvano, Shell elements with through-the-thickness variable kinematics for the analysis of laminated composite and sandwich structures, *Composites Part B: Engineering* 111 (2017) 294–314.
- [53] E. Carrera, M. Filippi, Variable kinematic one-dimensional finite elements for the analysis of rotors made of composite materials, *Journal of Engineering for Gas Turbines and Power* 136 (9) (2014) 092501.
- [54] K. Surana, S. Nguyen, Two-dimensional curved beam element with higher-order hierarchical transverse approximation for laminated composites, *Computers & Structures* 36 (3) (1990) 499–511.
- [55] J. F. Davalos, Y. Kim, E. J. Barbero, Analysis of laminated beams with a layer-wise constant shear theory, *Composite Structures* 28 (3) (1994) 241–253.
- [56] X. Lin, Y. Zhang, A novel one-dimensional two-node shear-flexible layered composite beam element, *Finite Elements in Analysis and Design* 47 (7) (2011) 676 – 682.
- [57] T. P. Vo, H.-T. Thai, Static behavior of composite beams using various refined shear deformation theories, *Composite Structures* 94 (8) (2012) 2513–2522.
- [58] E. Carrera, M. Filippi, P. K. Mahato, A. Pagani, Accurate static response of single- and multi-cell laminated box beams, *Composite Structures* 136 (2016) 372–383. doi:10.1016/j.compstruct.2015.10.020.